

# Charge pumping in monolayer graphene driven by a series of time-periodic potentials

Zhenhua Wu,<sup>1,2</sup> J. Li,<sup>3</sup> and K. S. Chan<sup>4</sup>

<sup>1</sup>*SKLSM, Institute of Semiconductors, Chinese Academy of Sciences,  
P.O. Box 912, 100083, Beijing, China*

<sup>2</sup>*CAE Team, Semiconductor R & D Center, Samsung Electronics Co., Ltd. Gyeonggi-Do, Korea\**

<sup>3</sup>*Department of Physics, Semiconductor Photonics Research Center, Xiamen University, Xiamen 361005, China*

<sup>4</sup>*Department of Physics and Materials Science,  
City University of Hong Kong,  
Tat Chee Avenue, Kowloon, Hong Kong, China†*

We applied the Floquet scattering-matrix formalism to studying the electronic transport properties in a mesoscopic Dirac system. Using the method, we investigate theoretically quantum pumping driven by a series of time-periodic potentials in graphene monolayer both in the adiabatic and non-adiabatic regimes. Our numerical results demonstrate that adding harmonic modulated potentials can break the time reversal symmetry when no voltage bias is applied to the graphene monolayer. Thus, when the system is pumped with proper dynamic parameters, these scatterers can produce a nonzero dc pumped current. We also find that the transmission is anisotropic as the incident angle is changed.

**Keywords:** graphene, pumping, Floquet scattering-matrix

PACS numbers: 72.10.-d, 73.20.-r, 73.23.-b, 73.40.Gk

## I. INTRODUCTION

Quantum transport in periodically driven mesoscopic systems is currently of great interest because of an increasing number of applications. [1–12] Many research studies have been carried out on the mechanism of scattering by time-dependent potentials in recent years. There exists a good theoretical understanding of the tunnelling events in the presence of an alternating (AC) field, i.e., the Floquet theory, [13–16] which takes the photon-assisted transport into account and allows us to convert the solution of a time-periodic Schrödinger equation into a time-independent eigenvalue problem. For systems with time-periodic potentials, inelastic tunnelling occurs when electrons at appropriate incident Fermi energies undergo transitions between the central band to several sidebands by means of photon emission or absorption, referred to as photon-assisted tunneling (PAT). The central band just corresponds to particles with the incident Fermi energy while the sidebands correspond to particles which have gained or lost one or more modulation energy quantum. Especially, if the potential is harmonic in time, the PAT results in exchange of energy with electrons in units of modulation quantum  $\hbar\omega$ , with  $\omega$  being the modulation frequency. An important application of the PAT is quantum charge pump, which received considerable theoretical investigation and had been observed experimentally.[2–5, 7–10, 15, 16] However most previous studies in this realm have been focused on the Schrödinger system.

In Ref.[16], the Floquet scattering theory was devel-

oped for quantum pumping in mesoscopic semiconductors by Moskalets and Büttiker. This approach permits description of both adiabatic and non-adiabatic regimes of pumping. It is the purpose of this work to applied the Floquet scattering-matrix method to calculating quantum charge pumping in the Dirac system. To this end, we extend the approach of Ref.[16] to accommodate a novel two dimensional hexagonal carbon material, graphene. Recently, the study of quantum pumps in Dirac system has been carried out in one dimensional Luttinger liquid model [17] or weak pumps in the adiabatic regime [18, 19] and nonadiabatic regime [20, 21] in graphene by using the Floquet scattering theory. Graphene, a single layer of carbon atoms arranged in a hexagonal lattice, exhibits abundant new physics and potential applications. [22–26] Quantum transport properties in graphene have attracted increasing attentions both for the fundamental physics and potential applications in carbon-based nanoelectronics devices. The novel properties arise from the unique linear dispersion and the chiral nature of its carriers near the Dirac points. At the  $K$  ( $K'$ ) point of the Brillouin zone, the energy spectrum exhibits a linear dispersion that can be well described by the massless Dirac equation with an effective speed of  $v_F \approx 10^6 m s^{-1}$ . [26] These quasiparticles, called massless Dirac fermions, are quite different from the standard electrons that we encounter in conventional two dimensional electron gases in semiconductor heterostructures. Graphene monolayer is a suitable testbed to examine the photon-assisted electron tunneling [27, 28] and quantum pumps in the Dirac system. In addition, the high electron mobility and long phase coherence present in graphene could in principle enhance these interference effects (photon-assisted tunneling and quantum pumps), thereby making possible its observation with the present technology. We carried out a study of quantum pumps in both adiabatic and non-

\*Electronic address: zhwu@semi.ac.cn, Tel.: +82-010-7287-1816

†Electronic address: apkschan@cityu.edu.hk

adiabatic regimes in graphene monolayer reported here, which helps to obtain a clear physical picture about time-dependent tunneling and will be interesting for the potential application of carbon-based electronic devices.

In this work, we study theoretically the charge pump by a series of time-periodic potentials in monolayer graphene with no external bias. We also find exchange of photons between the oscillating barrier and electrons. Such processes give rise to transitions from the central band to sidebands, all of which can convey the electrons and contribute to the pumped current. The charge pumping is a consequence of the interference of different propagating modes of which the differences in phase break the time reversal symmetry.

This paper is organized as follows. In Sec. II, we present the theoretical model and the calculation method. We show the numerical results and discussions in Sec. III. Finally, we give the conclusions in Sec. IV.

## II. THEORY

### A. Floquet scattering model in graphene

We consider electrons transmitting through a series of modulated pumping potentials in a monolayer graphene sheet. The charge pumping potentials can be realized by top metallic gates [29] or by using the electric field of a surface acoustic wave. [30] We approximate the scattering potentials by a sequence of time-periodic rectangular barriers. The barriers are infinite along the  $y$ -direction and homogeneous in each region as illustrated in Fig. 1. The potentials are given by:

$$V^i(\mathbf{r}, t) = V_0^i + V_1^i \cdot \cos(\omega t + \varphi^i), \quad (x_0^i < x < x_0^{i+1}), \quad (1)$$

where the superscript  $i$  indicates the  $i$ -th region (see Fig. 1). The height of the barrier is oscillating sinusoidally around  $V_0^i$  with amplitude  $V_1^i$ , frequency  $\omega$  and phase  $\varphi^i$ . Quasiparticles in graphene are formally described by the Dirac-like Hamiltonian:

$$\hat{H} = \hbar v_F \boldsymbol{\sigma} \cdot \mathbf{k} + V^i(\mathbf{r}, t). \quad (2)$$

where  $\mathbf{k}$  is the momentum,  $\sigma_i (i = x, y)$  is the pseudospin Pauli matrix, and the  $k$ -independent Fermi velocity  $v_F$  plays the role of the speed of light.

The Floquet theorem asserts that the solution of the eigen-energy problem in our system has the form:

$$\psi_F(\mathbf{r}, t) = e^{-iE_F t/\hbar} \phi(\mathbf{r}, t), \quad (3)$$

where  $E_F$  is the Floquet eigen-energy and  $\phi(\mathbf{r}, t) = \phi(\mathbf{r}, t+T)$  is a periodic function, with period  $T = 2\pi/\omega$ . Since the time and position dependence of  $V^i(\mathbf{r}, t)$  are separated in our model,  $\phi(\mathbf{r}, t)$  is separable as  $\phi(\mathbf{r}, t) = g(\mathbf{r})f(t)$ . This leads to the following equations for  $g(\mathbf{r})$  and  $f(t)$ , respectively:

$$-i\hbar v_F \boldsymbol{\sigma} \cdot \nabla g(\mathbf{r}) + V_0^i g(\mathbf{r}) = E g(\mathbf{r}), \quad (4)$$

$$i\hbar \frac{\partial}{\partial t} f(t) - V_1^i \cos(\omega t + \varphi^i) f(t) = (E - E_F) f(t), \quad (5)$$

where  $E$  is a constant. Integrating Eq. (5) gives:

$$\begin{aligned} f(t) &= e^{-i(E-E_F)t/\hbar} \exp\left(-\frac{i}{\hbar} \int_0^t V_1^i \cos(\omega t' + \varphi^i) dt'\right) \\ &= e^{-i(E-E_F)t/\hbar} \sum_{n=-\infty}^{n=\infty} J_n\left(\frac{V_1^i}{\hbar\omega}\right) e^{-in\omega t} e^{-in\varphi^i}, \end{aligned} \quad (6)$$

where we have taken  $f(0) = 1$ , and  $J_n$  is the Bessel function of the first kind in order  $n$ . Note that  $f(t) = f(t+T)$ , Eq. (6) requires that  $E = E_F + m\hbar\omega$ , where  $m$  is an integral index of the sidebands. The translational invariance along the  $y$  direction gives rise to the conservation of  $k_y$ , and thus the solutions can be written as  $g(\mathbf{r}) = g(x)e^{ik_y y}$ . The equation for  $g(\mathbf{r})$  has a solution:

$$\begin{aligned} g(\mathbf{r}) &= \sum_{m=-\infty}^{m=\infty} \left[ b_m^i \left( \frac{k_m^i + ik_y}{E_m^i} \right) e^{ik_m^i(x-x_0^i)} \right. \\ &\quad \left. + c_m^i \left( -\frac{k_m^i - ik_y}{E_m^i} \right) e^{-ik_m^i(x-x_0^i)} \right] e^{ik_y y}, \end{aligned} \quad (7)$$

where  $k_m^i = \text{sgn}(E_m^i) \sqrt{(E_m^i)^2 - (\hbar v_F k_y)^2}$  is the wavevector of the  $n$ -th sideband in the  $x$ -direction,  $\varphi^i$  is the phase of the oscillating potential in the  $i$ -th region. Note that, here  $E_m^i \equiv (E_F - V_0^i + m\hbar\omega)/(\hbar v_F)$  has the same dimension as the wavevectors  $k_m^i$  and  $k_y$ . According to Eq. 7, the Floquet energy  $E_F$  can be determined up to an arbitrary integer multiplied by  $\hbar\omega$ . We can define  $E_0 \equiv E_F$ ,  $E_n \equiv E_F + n\hbar\omega$ . By combining the the solutions for  $f(t)$  and  $g(\mathbf{r})$ , we can write the solution for the Floquet state as:

$$\begin{aligned} \phi(x, t) &= \sum_{m=-\infty}^{m=\infty} \sum_{n=-\infty}^{n=\infty} \left[ b_m^i \left( \frac{k_m^i + ik_y}{E_m^i} \right) e^{ik_m^i(x-x_0^i)} \right. \\ &\quad \left. + c_m^i \left( -\frac{k_m^i - ik_y}{E_m^i} \right) e^{-ik_m^i(x-x_0^i)} \right] J_{n-m}\left(\frac{V_1^i}{\hbar\omega}\right) \\ &\quad \cdot e^{-i(n-m)\varphi^i} e^{-i(E_0+n\hbar\omega)t/\hbar} e^{ik_y y}. \end{aligned} \quad (8)$$

Note that, in the free region, i.e.,  $V_1^i = 0$ ,  $J_{n-m}(0) = \delta_{m,n}$  and Eq. (8) can also describe the electronic states correctly. Here we have obtained the wave functions that valid both in the free and oscillating regions in a unified form. Then we can use Floquet scattering-matrix formalism (see Appendix. A) to calculate the pumped current.

### B. Pumped current

Using the distribution function  $f_\alpha^{\text{out}}(E)$  for outgoing particles and  $f_\alpha^{\text{in}}(E)$  for incoming ones, we can find the directed current  $I_\alpha$  in the lead  $\alpha$ :

$$I_\alpha = \frac{eL_y}{\pi\hbar} \int_{-\infty}^{\infty} \int_{-E/\hbar v_F}^{E/\hbar v_F} dE dk_y \{ f_\alpha^{\text{out}}(E) - f_\alpha^{\text{in}}(E) \}, \quad (9)$$

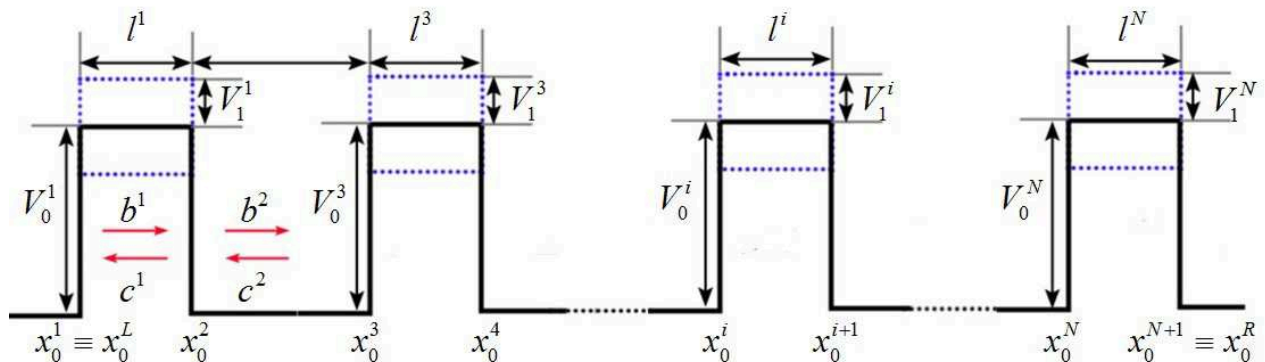


FIG. 1: Schematic diagram of a series of time-periodic potentials.

where, the  $f_\alpha^{\text{out}}(E)$  can be calculated by using the S-matrix  $S_F$  that we have already obtained in Appendix. A:

$$f_\alpha^{\text{out}}(E) = \sum_\beta \sum_{\text{pro-n}} |S_{F,\alpha\beta}(E, E_n)|^2 f_\beta^{\text{in}}(E_n). \quad (10)$$

The subscript *pro-n* indicates that the second summation in Eq. (10) only includes the propagating states with real wave vectors that contribute to the current. The bound states near the oscillating scatterer are neglected for electrons in these states are confined around the boundaries without transmitting far away. Substituting Eq. (10) into Eq. (9), we have:

$$I_\alpha = \frac{eL_y}{\pi\hbar} \int_{-\infty}^{\infty} \int_{-E/hv_F}^{E/hv_F} dE dk_y \sum_\beta \sum_{\text{pro-n}} |S_{F,\alpha\beta}(E, E_n)|^2 (f_\beta^{\text{in}}(E_n) - f_\alpha^{\text{in}}(E)). \quad (11)$$

The pumped current at the low temperature limit is:

$$I_\alpha = \frac{eL_y}{\pi\hbar} \int_{E_{Fermi}-N\hbar\omega}^{E_{Fermi}+N\hbar\omega} \int_{-E/hv_F}^{E/hv_F} dE dk_y \sum_\beta \sum_{\text{pro-n}} |S_{F,\alpha\beta}(E, E_n)|^2 (f_\beta^{\text{in}}(E_n) - f_\alpha^{\text{in}}(E)), \quad (12)$$

where,  $\alpha$  is the outgoing terminal,  $\beta$  is the incoming terminal,  $N$  is the maximum index of the sidebands that need to be included in the calculation and it is determined by the amplitude and frequency of the oscillation (proportional to  $V_1/\hbar\omega$ ). Next we consider the adiabatic limitation:  $\omega \rightarrow 0$ . In this situation, the Floquet scattering matrix is almost energy independent when  $E$  changes by  $N\hbar\omega$ . We can rewrite the Floquet scattering matrix in adiabatic approximation as  $S_{F,\alpha\beta}(E, E_n) \rightarrow S_{0,\alpha\beta,n}(E)$ , and the difference of the Fermi distribution as  $f(E_n) - f(E) = n\hbar\omega \frac{f(E_n) - f(E)}{E_n - E} \rightarrow n\hbar\omega \frac{\partial f_0(E)}{\partial E}$ , where  $n$  denotes the  $n$ -th sideband in which the electrons are scattered to. Inserting the above expressions into Eq. (11), the pumped current in the adiabatic pumping regime can

be reduced to,

$$I_\alpha = \frac{eL_y\omega}{2\pi^2} \int_{-\infty}^{\infty} \int_{-E/hv_F}^{E/hv_F} dE dk_y \sum_\beta \sum_{\text{pro-n}} n |S_{0,\alpha\beta,n}(E)|^2 \frac{\partial f_0(E)}{\partial E}. \quad (13)$$

We note en passant that, at the low temperature limit, only the particles close to the Fermi level can contribute to the adiabatic pumped current as indicated by the derivative of the Fermi distribution in Eq. (13). We can also use the scattering matrix to calculate some other important physical quantities such as the directed heat current, shot noise, Wigner delay time. [9, 14–16]

### III. NUMERICAL RESULTS AND DISCUSSIONS

#### A. Transmission asymmetry

In this section, we use the above formalism to investigate quantum tunneling through double oscillating barriers schematically illustrated in Fig. 1 with only the first two oscillating barriers included. It is clear that a single time-periodic barrier with time-reversal symmetry can not produce a pumped current. Here we consider only two oscillating potentials which are sufficient to present a clear physical picture. The heights of the two barriers oscillate in time with the same frequency  $\omega$ , amplitude  $V_1$ , but with a phase lag  $\Delta\varphi$ . Thus for a pump with  $\Delta\varphi \neq n\pi$  ( $n$  is an integer), the time-reversal symmetry is broken and a nonzero pumped current can be produced. To understand the origin of the directed current when the chemical potentials at both sides of the scatterers are equal, we first examine the transmission asymmetry for incoming waves in a certain mode  $E_0 = E$  from both sides of the scattering region.

$$T_{net} = \sum_{pro-n} \left\{ |S_{F,\alpha\beta}(E_n, E)|^2 \frac{v_n^\alpha}{v_0} f_\beta^{in}(E) - |S_{F,\beta\alpha}(E_n, E)|^2 \frac{v_n^\beta}{v_0} f_\alpha^{in}(E) \right\}, \quad (14)$$

where  $\alpha$  denotes the right terminal and  $\beta$  denotes the left terminal.

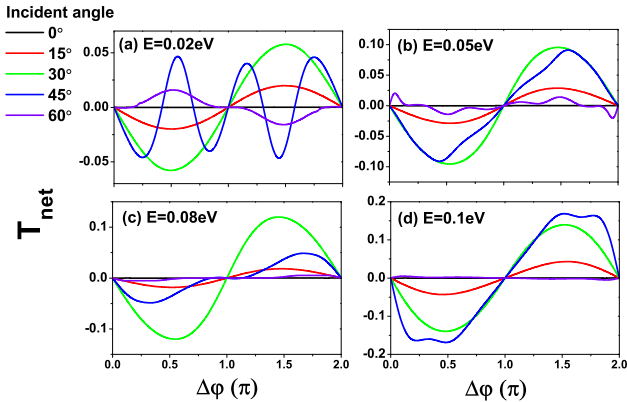


FIG. 2: The transmission asymmetry as a function of the phase lag  $\Delta\varphi$  at different incident angles and energies, with  $V_0 = 200$  meV,  $V_1 = 9$  meV,  $\hbar\omega = 3$  meV,  $l_1 = l_3 = 50$  nm  $l_2 = 25$  nm

In Fig. 2, we plot the transmission asymmetry probability as a function of the phase lag  $\Delta\varphi$  at different incident angles and energies. Anisotropic tunneling behavior is observed in this time-periodic case. Note that for normal incidence,  $T_{net}$  is always zero. This phenomena is the result of Klein tunneling i.e., the incident electrons at both sides of the scatterer can perfectly transmit to the opposite side resulting in the vanish of the transmission asymmetry. In Fig. 3(a)-(c), we present the transmission asymmetry probability as a function of incident energy under a certain Fermi energy  $E_F = 0.2$  eV, while the widths of the barriers are different. Our calculation shows that  $T_{net}$  vanishes gradually as the incident energy decreases, since the influence of the oscillating potentials that break the time-reversal symmetry become negligible when the incident energy is far below  $V_0$  as well as the oscillating potentials. The transmission asymmetry probability oscillates more seriously when the barrier is thicker by comparing Fig. 3(a)-(c). This is related to the interference between the multireflections of the electron waves inside the barriers. So it shows more pronounced resonant tunneling behaviors as the barrier width increases. We also investigate the effect of the oscillating amplitude  $V_1$  and frequency  $\omega$  on  $T_{net}$  as shown in Fig. 3(d)-(f). We find that the transmission asymmetry probability can be enlarged both by increasing  $V_1$  or  $\omega$  for small values of  $\omega$ . Such results are obvious since larger  $V_1$  gives rise to a greater number of sidebands serving as the transmission modes, while larger  $\omega$  gives rise

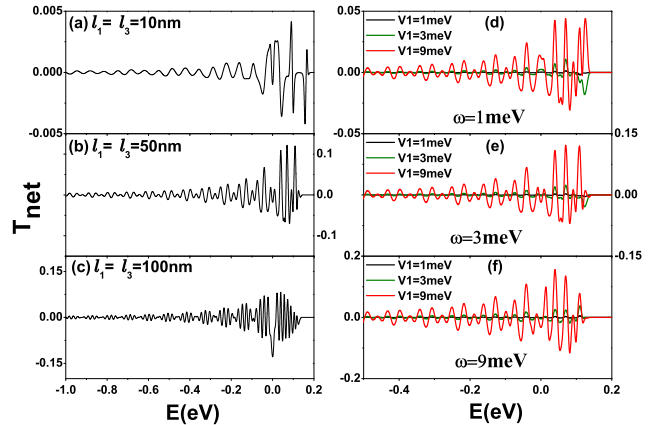


FIG. 3: (a)-(c) The transmission asymmetry  $T_{net}$  as a function of incident energy with different barrier widths.  $V_0 = 200$  meV,  $V_1 = 9$  meV,  $\hbar\omega = 3$  meV. (d)-(f) The transmission asymmetry  $T_{net}$  as a function of incident energy with different amplitudes and frequency of the oscillating potentials.  $l_1 = l_3 = 50$  nm,  $V_0 = 200$  meV. In all panels the incident angle and the distance between the two barriers are fixed, i.e.,  $\phi = 30^\circ$ ,  $l_2 = 25$  nm.

to larger modulation quantum of energy that an electron exchanged with the oscillating potentials during the tunneling processes. In Fig. 3, we find that the transmission asymmetry vanishes when the incident energy approaches  $V_0$ . This is because the  $x$ -component of the wave vector  $k_m$  of the central band and first few sidebands in the barrier are imaginary in the incident energy range closed to  $V_0$ . Imaginary wave vectors corresponds to evanescent modes, that decay exponentially and thus lead to total reflection at both sides of the scatterer. [32] The breaking of the time-reversal symmetry by the interference of different traversal modes (i.e., central band and sidebands) is attributed to the phase lag between the two oscillating potentials.

## B. Adiabatic Pumped Current

Nonzero transmission asymmetry can give rise to a finite charge current. Next we proceed to calculate the pumped current in adiabatic limit:  $\omega \rightarrow 0$ . The expression of adiabatic pumped current in Eq. (13) is valid when the Floquet scattering matrix is energy independent on the scale of the order of  $N\hbar\omega$ . The larger the number  $N$  of the sidebands included, the smaller the frequencies for which the adiabatic approximation is valid. As discussed above,  $N$  is determined by the ratio of the oscillation amplitude to the frequency. In this subsection, we consider a weak pump with  $N = 3$ . For a strong pump,  $N$  is much larger and the adiabatic approximation is valid only at smaller frequencies. In Fig. 3, we can see that the transmission asymmetry shows a resonance-like behavior

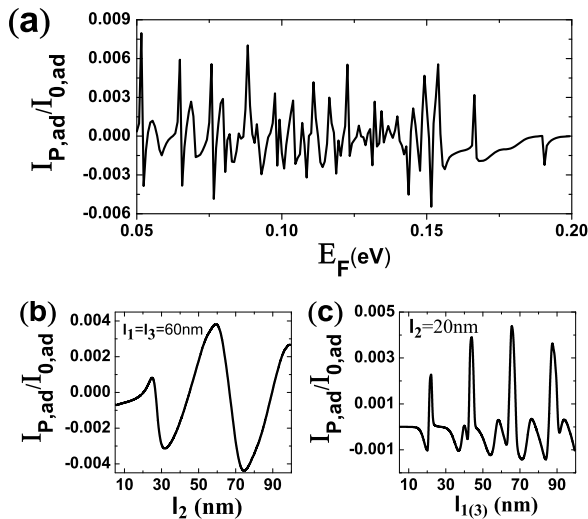


FIG. 4: (a) Energy dependence of the adiabatic pumped current, with  $\Delta\varphi = \pi/2$ ,  $\omega = 0.03$  meV,  $V_1 = 3\omega$ ,  $V_0 = 0.2$  eV  $l_2 = 60$  nm,  $l_1 = l_3 = 100$  nm, and  $I_{0,ad} \equiv eL_y\omega/(2\pi^2)$ . (b)-(c) The adiabatic pumped currents versus the barrier separation and barrier width for fixed Fermi energy  $E_F = 80$  meV.

of the order of the width  $\delta E \sim 0.02$  eV resonance, indicating that the Floquet scattering matrix changes significantly over this energy scale. Therefore we can choose an oscillating frequency of  $\omega = 0.03$  meV, for which the adiabatic approximation requirement  $N\hbar\omega \ll \delta E$  is satisfied. Note that at zero temperature the pumped current is dominated by the electrons at the Fermi energy. The pumped current  $I_{P,ad}$  shows similar resonance-like behaviors as transmission asymmetry as expected (see Fig. 4(a)).  $I_{P,ad}$  oscillates as a function of the Fermi energy  $E_F$ , becomes smooth and eventually vanishes when the fermi energy approaches the static potential height  $V_0$ . It is much different from that of a conventional quantum pump based on usual nano-scale semiconductors. This remarkable feature can be attributed to the same reason as the vanished transmission asymmetry when  $E_F$  is close to  $V_0$  as we examined in the last subsection, i.e., the transmission probability in graphene through a high barrier is larger than that of a low barrier which is closed to the incident energy. Another difference between the quantum pumps in graphene and that in the conventional two-dimensional electron gas system is that the pumped current in graphene can change from positive to negative or reversely as the energy increases for a constant phase lag, while the direction of conventional pumped current is determined by the phase lag of the to oscillating potentials. [19] We also investigated the influence of the geometrical sizes of the oscillating double barriers. In Figs. 4(b) and (c), we plot the dependence of adiabatic pumped currents both on the barrier separation  $l_2$  and width  $l_{1(3)}$ . The adiabatic pumped current also oscillates when the barrier separation or width are changed. This is caused by the Fabry-Pérot resonant

modes formed between the interfaces due to the multiple reflections. [11] These results agree with the previous work on adiabatic pumping in graphene, e.g. see [19]. With increasing pumped frequency, the deviation of the actual pumped current calculated by Eq.(12) from the adiabatic one calculated by Eq.(13) becomes significant, and thus the adiabatic approximation of Eq.(13) as well as the parametric scattering approach used in Ref.[19] are not valid anymore.

### C. Non-adiabatic Pumped Current

Next, we analyze the behavior of non-adiabatic pumped current  $I_P$  as a function of phase lag  $\Delta\varphi$  by using Eq. (12). The incident electrons are homogeneous in direction under the same Fermi energy  $E_F$  from both sides of the scatterer. Fig. 5(a) shows the general characteristics of quantum pumping in graphene. The oscillating frequency is set to  $\omega = 3$  meV, and thus  $N\hbar\omega$  is of the same order of  $\delta E$ . The adiabatic approximation discussed in last subsection is no longer valid. The sizes of the double oscillating barriers are fixed for  $l_2 = 25$  nm,  $l_1 = l_3 = 50$  nm in the calculation of this subsection. The numerical results show that the pumped current  $I_P$  is sinusoidal or cosinoidal dependence on phase lag  $\Delta\varphi$ . We find that the static barrier  $V_0^i$  can also effectively control the amplitude and direction of the current as shown in Fig. 5(b). The height of the static barrier  $V_0^i$  plays an important role in determining the pumping, since it is related to the component of the wave vector along the x-direction in the barrier region. For electron in the  $n$ -th energy sideband  $|E + n\hbar\omega - V_0^i| < \hbar v_F k_y$ , the corresponding  $x$ -component of the wave vector  $k_n^i$  becomes imaginary. Such electrons are in evanescent sidebands and do not directly contribute to the current. If the static barrier becomes higher, the electronic states outside the barrier match the hole states inside the barrier. Then the transmission modes in the barrier come back to propagating states, resulting in an increasing overall pumped current amplitude. This phenomena in graphene is different from the transmission in ordinary semiconductor two dimensional electron gas, while there is no available hole state inside the barrier contributing to ordinary tunneling. One can see in Fig. 5(b) that the pumped current oscillates when the static barrier potential is increased. This is caused by the Fabry-Pérot resonant modes formed in the double barrier structure due to the multiple reflections. [11]

The pumped current can also be tuned by the oscillating amplitude  $V_1$  and frequency  $\omega$  as shown in Fig. 6. We find that the pumped current increases with the oscillating amplitude  $V_1$ . This is because a larger  $V_1$  can transfer electrons to higher sidebands and thus increase the transmission modes of which the interferences become more intensive. This behavior is much different from that of an adiabatic pump. In the limit of  $\omega \rightarrow 0$ , the adiabatic pumped current is irrespective of the amplitude

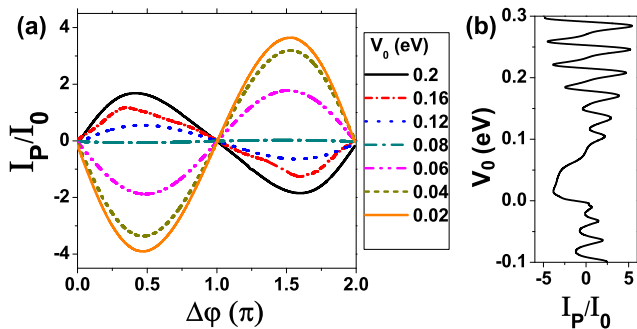


FIG. 5: (a) The pumped currents versus the phase lag  $\Delta\varphi$  for different  $V_0$ , with  $E_F = 80$  meV,  $\omega = 3$  meV,  $V_1 = 9$  meV,  $I_0 \equiv eL_y/(10^5 \pi h)$ . (b) The pumped currents versus  $V_0$ , with  $\Delta\varphi = \pi/2$ .

of the oscillating potentials  $V_1$ , however the criterion of adiabatic approximation depends strongly on  $V_1$ . [16]

In Fig. 6(b), we inspect the influence of the frequency  $\omega$  for several fixed amplitude  $V_1$ . The pumped current shows a trend of rise first, then fall after  $\omega$  exceeding  $V_1$ . For small  $\omega$ , electrons can gain a larger modulation energy quantum from the oscillating potentials with increasing  $\omega$ . The interference of sidebands with higher energies gives rise to a larger pumped current. With increasing pumped frequency  $\omega$  under a constant oscillating potential  $V_1$ , the oscillating double barriers will transform from a strong pump to a weak pump. In the case that  $\omega$  is larger than  $V_1$ , the oscillating pump is too weak to lift the electrons from the central band to any sidebands and thus leads to the drop of the pumped current. This feature does not exist in adiabatic pumping regimes, since the pumped frequency  $\omega$  is always much smaller than the oscillating potential  $V_1$ , and the adiabatic current always increases monotonely with  $\omega$ . [17] Therefore, the non-adiabatic pumped current can be tuned by changing the phase lag, barrier height, oscillating amplitude and frequency.

#### IV. CONCLUSION

In summary, we applied the iterative Floquet scattering-matrix method to the Dirac system, which is able to calculate the pumped current induced by an arbitrary number of parametric oscillating potentials between two electron reservoirs without external bias. Based on this approach, we investigate theoretically the quantum pumping driven by a series of time-periodic potentials in graphene monolayer both in adiabatic and non-adiabatic regimes. We have determined how the pumped current depends on the phase lag, height of the barrier, frequency and amplitude of the oscillation. Finally, the physical mechanism of quantum pumping is attributed to the interference of different central band and sidebands of which the phases factor break the time reversal symme-

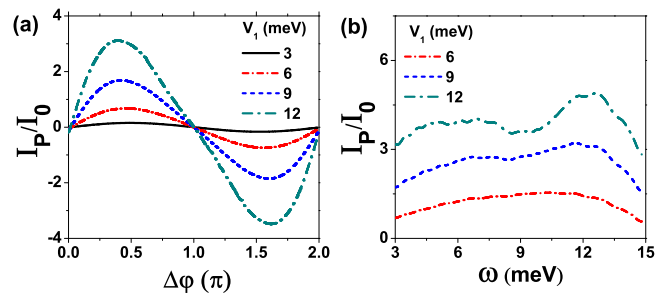


FIG. 6: (a) The pumped currents versus the phase lag  $\Delta\varphi$  for different  $V_1$ , with  $E_F = 80$  meV,  $\omega = 3$  meV,  $V_0 = 200$  meV,  $I_0 \equiv eL_y/(10^5 \pi h)$ . (b) The pumped currents versus  $\omega$ , with  $\Delta\varphi = \pi/2$ .

try.

#### Acknowledgments

The work described in this paper was supported by the Collaborative Research Fund of the Research Grants Council of Hong Kong SAR, China under Project No. CityU5/CRF/08 and NSFC Grant No.11104232.

#### Appendix A: Transfer-matrix and Scattering-matrix

In Sec. II A, we have obtained the wave functions for all the free and oscillating regions. The wave functions (see Eq. (8)) must be continuous at each boundary  $x = x_0^{0,1,2,\dots}$ . At the boundary between region  $i$  and  $i+1$  ( $x = x_0^{i+1}$ ), the coefficients matrices can be related by the transfer matrix  $\mathbf{M}(i, i+1)$ ,

$$\begin{pmatrix} B^i \\ C^i \end{pmatrix} = \mathbf{M}(i, i+1) \begin{pmatrix} B^{i+1} \\ C^{i+1} \end{pmatrix}, \quad (\text{A1})$$

where  $\mathbf{B}$  ( $\mathbf{C}$ ) is the probability amplitudes column vector of the right(left)-going waves (see Fig. 1). Matching the wavefunctions at  $x_0^{i+1}$  and realizing that  $e^{-i(E_0+n\hbar\omega)t/\hbar}$  with different  $n$  are orthogonal, we have:

$$\begin{aligned} & \sum_n \sum_m J_{n-m} \left( \frac{V_1^i}{\hbar\omega} \right) \cdot e^{-i(n-m)\varphi^i} [b_m^i e^{ik_m^i l^i} + c_m^i e^{-ik_m^i l^i}] \\ &= \sum_n \sum_m J_{n-m} \left( \frac{V_1^{i+1}}{\hbar\omega} \right) \cdot e^{-i(n-m)\varphi^{i+1}} [b_m^{i+1} + c_m^{i+1}], \quad (\text{A2}) \end{aligned}$$

and

$$\begin{aligned}
& \sum_n \sum_m J_{n-m} \left( \frac{V_1^i}{\hbar\omega} \right) \cdot e^{-i(n-m)\varphi^i} \\
& \cdot \left[ \frac{k_m^i + \mathbf{i}k_y}{E_m^i} \cdot b_m^i e^{ik_m^i l^i} - \frac{k_m^i - \mathbf{i}k_y}{E_m^i} \cdot c_m^i e^{-ik_m^i l^i} \right] \\
& = \sum_n \sum_m J_{n-m} \left( \frac{V_1^{i+1}}{\hbar\omega} \right) \cdot e^{-i(n-m)\varphi^{i+1}} \\
& \cdot \left[ \frac{k_m^{i+1} + \mathbf{i}k_y}{E_m^{i+1}} \cdot b_m^{i+1} - \frac{k_m^{i+1} - \mathbf{i}k_y}{E_m^{i+1}} \cdot c_m^{i+1} \right], \quad (\text{A3})
\end{aligned}$$

where,  $l^i = x_0^{i+1} - x_0^i$ , is the distance of the  $i$ -th region. In order to convert the above two equations into the matrix form, we define:

$$(\gamma^i)_{nm} \equiv e^{ik_m^i l^i} \cdot \delta_{mn}; \quad (\text{A4})$$

$$(P^i)_{nm} \equiv J_{n-m} \left( \frac{V_1^i}{\hbar\omega} \right) \cdot e^{-i(n-m)\varphi^i}; \quad (\text{A5})$$

$$(Q_R^i)_{nm} \equiv J_{n-m} \left( \frac{V_1^i}{\hbar\omega} \right) \cdot e^{-i(n-m)\varphi^i} \cdot \left( \frac{k_m^i + \mathbf{i}k_y}{E_m^i} \right); \quad (\text{A6})$$

$$(Q_L^i)_{nm} \equiv J_{n-m} \left( \frac{V_1^i}{\hbar\omega} \right) \cdot e^{-i(n-m)\varphi^i} \cdot \left( -\frac{k_m^i - \mathbf{i}k_y}{E_m^i} \right). \quad (\text{A7})$$

Using the boundary conditions Eq. (A2) and Eq. (A3) we can obtain the transfer matrix:

$$\begin{aligned}
\mathbf{M}(i, i+1) & = \begin{pmatrix} \gamma^i & 0 \\ 0 & (\gamma^i)^{-1} \end{pmatrix}^{-1} \begin{pmatrix} P^i & P^i \\ Q_R^i & Q_L^i \end{pmatrix}^{-1} \\
& \cdot \begin{pmatrix} P^{i+1} & P^{i+1} \\ Q_R^{i+1} & Q_L^{i+1} \end{pmatrix}. \quad (\text{A8})
\end{aligned}$$

If we define:

$$T(i, i+1) \equiv \begin{pmatrix} P^i & P^i \\ Q_R^i & Q_L^i \end{pmatrix}^{-1} \begin{pmatrix} P^{i+1} & P^{i+1} \\ Q_R^{i+1} & Q_L^{i+1} \end{pmatrix}, \quad (\text{A9})$$

we have all the four sub-transfer matrix:

$$\begin{aligned}
M_{11}(i, i+1) & = (\gamma^i)^{-1} T_{11}(i, i+1), \\
M_{12}(i, i+1) & = (\gamma^i)^{-1} T_{12}(i, i+1), \\
M_{21}(i, i+1) & = (\gamma^i) T_{21}(i, i+1), \\
M_{22}(i, i+1) & = (\gamma^i) T_{22}(i, i+1). \quad (\text{A10})
\end{aligned}$$

So far, we have obtained the transfer matrices of each region. But for an evanescent mode, where  $k_m^i$  becomes imaginary, the  $(\gamma^i)_{mm}$  and  $(\gamma^i)_{mm}^{-1}$  will, respectively, decay or grow exponentially. An approach to avoid this problem is using the scattering matrix formalism. In the following, we obtain the scattering matrix for the graphene system following Xu's work on quantum antidot arrays. [31]

The scattering matrix  $S(L, R)$ , connecting the incoming and outgoing channels, is defined as follows:

$$\begin{aligned}
\begin{pmatrix} B^R \\ C^L \end{pmatrix} & = S(L, R) \begin{pmatrix} B^L \\ C^R \end{pmatrix} \\
& \equiv \begin{pmatrix} S_{11}(L, R) & S_{12}(L, R) \\ S_{21}(L, R) & S_{22}(L, R) \end{pmatrix} \begin{pmatrix} B^L \\ C^R \end{pmatrix}. \quad (\text{A11})
\end{aligned}$$

Then, we use the iterative scheme, if we already have  $S(L, i)$ :

$$\begin{pmatrix} B^i \\ C^L \end{pmatrix} = S(L, i) \begin{pmatrix} B^L \\ C^i \end{pmatrix}, \quad (\text{A12})$$

with the help of the transfer matrix (see Eq. (A1)), we can obtain the scattering matrix of the next boundary  $S(L, i+1)$ :

$$\begin{aligned}
S_{11}(L, i+1) & = [1 - M_{11}^{-1}(i, i+1)S_{12}(L, i)M_{21}(i, i+1)]^{-1} \\
& \cdot M_{11}^{-1}(i, i+1)S_{11}(L, i) \\
S_{12}(L, i+1) & = [1 - M_{11}^{-1}(i, i+1)S_{12}(L, i)M_{21}(i, i+1)]^{-1} \\
& \cdot M_{11}^{-1}(i, i+1)S_{12}(L, i)M_{22}(i, i+1) \\
& - M_{11}^{-1}(i, i+1)M_{12}(i, i+1)] \\
S_{12}(L, i+1) & = S_{22}(L, i)M_{21}(i, i+1)S_{11}(L, i+1) \\
& + S_{21}(L, i) \\
S_{22}(L, i+1) & = S_{22}(L, i)M_{21}(i, i+1)S_{12}(L, i+1) \\
& + S_{22}(L, i) \cdot M_{22}(i, i+1). \quad (\text{A13})
\end{aligned}$$

We have obtained the iterative relations of the scatter-matrices in Eq. (A13). It is easy to write the initial S-matrix:  $S_{L,L} = \hat{I}$ . Then we can get every desired S-matrix  $S_{L,R}$  using the iterative scheme step by step. Note that the current associated with a scattered wave is proportional to the square of the wavefunction multiplied by the velocity. In order to ensure current conservation The unitary Floquet scattering matrix by incorporating the velocities of different modes in the incident and outgoing terminals,

$$S_{F,\alpha\beta}(m, n) = S_{\alpha\beta}(m, n) \left| \frac{v_m^\alpha}{v_n^\beta} \right|^2, \quad (\text{A14})$$

where  $\alpha$  and  $\beta$  denote the terminals,  $m$  and  $n$  label the transmission modes. In this research of a series of time-periodic potentials, the velocities in the propagating direction is calculated as follows:

$$v_m^\alpha = \frac{1}{\hbar} \frac{\partial}{\partial k_m^\alpha} (\hbar v_F E_m^\alpha(k_m^\alpha, k_y)) = \frac{v_F k_m^\alpha}{E_m^\alpha}. \quad (\text{A15})$$

This iterative scattering-matrix method has the advantage that we can effectively investigate a complicate system consisting of an arbitrary number of parametric pumping regions even though evanescent modes may exist in such regions.

- 
- [1] M. Büttiker and R. Landauer, Phys. Rev. Lett. **49**, 1739 (1982).
- [2] M. Switkes, C. M. Marcus, K. Campman, and A. C. Gosard, *Science*. **283**, 1905 (1999).
- [3] D. J. Thouless, Phys. Rev. B **27**, 6083 (1983).
- [4] Q. Niu, Phys. Rev. Lett. **64**, 1812 (1990).
- [5] M. Wagner, Phys. Rev. B **49**, 16544 (1994); Phys. Rev. Lett. **76**, 4010 (1996); Phys. Rev. Lett. **85**, 174 (2000).
- [6] G. Burmeister, K. Maschke, Phys. Rev. B **57**, 13050 (1998).
- [7] P. W. Brouwer, Phys. Rev. B **58**, R10135 (1998); Phys. Rev. B **63**, 121303 (2001); M. L. Polianski and P. W. Brouwer, Phys. Rev. B **64**, 075304 (2001).
- [8] B. G. Wang, J. Wang, and H. Guo, Phys. Rev. B **65**, 073306 (2002).
- [9] S. L. Zhu, Z. D. Wang, Phys. Rev. B **65**, 155313 (2002).
- [10] L. E. F. Foa Torres, Phys. Rev. B **72**, 245339 (2005).
- [11] L. E. F. Foa Torres and G. Cuniberti, Appl. Phys. Lett. **94**, 222103 (2009); L. E. F. Foa Torres and G. Cuniberti, *C. R. Physique* **10**, 297 (2009); and C. G. Rocha, L. E. F. Foa Torres and G. Cuniberti, Phys. Rev. B **81**, 115435 (2010).
- [12] P. H. Rivera, A. L. C. Pereira, and P. A. Schulz, Phys. Rev. B **79**, 205406 (2009).
- [13] J. H. Shirley, Phys. Rev. **138**, B979 (1965).
- [14] W. Li, L. E. Reichl, Phys. Rev. B **60**, 15732 (1999).
- [15] M. Moskalets and M. Büttiker, Phys. Rev. B **66**, 035306 (2002).
- [16] M. Moskalets and M. Büttiker, Phys. Rev. B **66**, 205320 (2002).
- [17] A. Agarwal and D. Sen, Phys. Rev. B **76**, 035308 (2007).
- [18] E. Prada, P. San-Jose, and H. Schomerus, Phys. Rev. B **80**, 245414 (2009).
- [19] R. Zhu and H. Chen, Appl. Phys. Lett. **95**, 122111 (2009).
- [20] P. San-Jose, E. Prada, S. Kohler, and H. Schomerus, Phys. Rev. B **84**, 155408 (2011).
- [21] L. E. F. Foa Torres, H. L. Calvo, C. G. Rocha, and G. Cuniberti, Appl. Phys. Lett. **99**, 092102 (2011).
- [22] K. S. Novoselov, A. K. Geim, S. V. Morozov, D. Jiang, Y. Zhang, S. V. Dubonos, I. V. Grigorieva, and A. A. Firsov, *Science* **306**, 666 (2004).
- [23] Y. Zhang, Y. Tan, H. L. Stormer, and P. Kim, *Nature* **438**, 201 (2005).
- [24] K. S. Novoselov, Z. Jiang, Y. Zhang, S. V. Morozov, H. L. Stormer, U. Zeitler, J. C. Maan, G. S. Boebinger, P. Kim, and A. K. Geim, *Science* **315**, 1379 (2007).
- [25] A. K. Geim, and K. S. Novoselov, *Nature Mater.* **6**, 183 (2007).
- [26] A. H. Castro Neto, F. Guinea, N. M. R. Peres, K. S. Novoselov, and A. K. Geim, *Rev. Mod. Phys.* **81**, 109 (2009).
- [27] B. Trauzettel, Ya. M. Blanter, and A. F. Morpurgo, Phys. Rev. B **75**, 035305 (2007).
- [28] M. A. Zeb, K. Sabeeh, M. Tahir, Phys. Rev. B **78**, 165420 (2008).
- [29] H. Schomerus, Phys. Rev. B **76**, 045433 (2007).
- [30] M. R. Buitelaar, V. Kashcheyevs, P. J. Leek, V. I. Talyanskii, C. G. Smith, D. Anderson, G. A. C. Jones, J. Wei, and D. H. Cobden, Phys. Rev. Lett. **101**, 126803 (2008).
- [31] H. Q. Xu, Phys. Rev. B **50**, 8469 (1994).
- [32] Z. H. Wu, K. Chang, J. T. Liu, X. J. Li, and K. S. Chan, *J. Appl. Phys.* **105**, 043702 (2009).